Current Topics

Biomimetic Chemistry of Iron, Nickel, Molybdenum, and Tungsten in Sulfur-Ligated Protein Sites[†]

Stanislav Groysman and R. H. Holm*

Department of Chemistry and Chemical Biology, Harvard University, Cambridge, Massachusetts 02138

Received January 12, 2009; Revised Manuscript Received February 7, 2009

ABSTRACT: Biomimetic inorganic chemistry has as its primary goal the synthesis of molecules that approach or achieve the structures, oxidation states, and electronic and reactivity features of native metal-containing sites of variant nuclearity. Comparison of properties of accurate analogues and these sites ideally provides insight into the influence of protein structure and environment on intrinsic properties as represented by the analogue. For polynuclear sites in particular, the goal provides a formidable challenge for, with the exception of iron−sulfur clusters, all such site structures have never been achieved and few have even been closely approximated by chemical synthesis. This account describes the current status of the synthetic analogue approach as applied to the mononuclear sites in certain molybdoenzymes and the polynuclear sites in hydrogenases, nitrogenase, and carbon monoxide dehydrogenases.

SYNTHETIC ANALOGUES

A strategy of demonstrated value in the study of protein-bound metal sites is the synthetic analogue or biomimetic approach defined by the protocol of Figure 1 (*1*). As developed and implemented in this laboratory, this approach has as its objective the preparation and detailed characterization of relatively small molecules that simulate or achieve the coordination sphere, composition, stereochemistry, and oxidation states of the native metal mononuclear or polynuclear site. A structural analogue allows deduction of site characteristics common to the site and itself by property comparisons. A functional analogue supports substrate transformations to products as do enzymes, although not necessarily at the same rate or with the same stereochemistry. A functional analogue is not inevitably a structural analogue, but a high-fidelity structural analogue should be a functional analogue provided a protein environment is not obligatory to reactivity. The approach is iterative to improve as necessary the accuracy of a site analogue. Here we describe the current status of selected biomimetic chemistry of four metals (Fe, Ni, Mo, and W) in relation to proteins that are the objects of widespread contemporary interest: molybdenum and tungsten oxotransferases and hydroxylases, iron and nickel−iron hydrogenases, iron−sulfur proteins, molybdenum−copper and nickel−iron−sulfur carbon monoxide dehydrogenases, and nitrogenase. The sites in these proteins exhibit a range of metal nuclearities and have the common features of variable oxidation states and sulfur-rich coordination environments. Space limitations do not allow detailed accounts of enzyme reactions and mechanisms, protein structure, and inclusion of all meritorious results in site modeling. The emphasis is on the native sites themselves and recent synthetic inorganic chemistry directed toward meaningful analogues of those sites. More extensive accounts of the biomimetic chemistry of metalloprotein sites are available (*2, 3*).

MOLYBDENUM/TUNGSTEN OXOTRANSFERASES AND HYDROXYLASES

These enzymes catalyze overall reaction 1 in which generalized substrate X/XO is converted to product XO/X by addition or removal of one oxygen atom whose ultimate source is water (*4*−*7*).

$$X + H_2O \leftrightarrow XO + 2H^+ + 2e^- \quad (1)$$

Current interpretation of function derives substantially from more than 30 crystal structures of enzymes that catalyze more than a dozen different reactions. Molybdoenzymes are effectively organized under the Hille classification, which is partly based on the structures of oxidized (Mo^{VI}) active sites and includes the DMSOR,[1] SO, and XOR families (*4*). Active site structures in the DMSOR family (Figure 2)

[†] Research in this laboratory is supported by NIH Grant GM 28856 and NSF Grant CHE 00547734.

* To whom correspondence should be addressed: Department of Chemistry and Chemical Biology, Harvard University, 12 Oxford St., Cambridge, MA 02138. Phone: (617) 495-0853. Fax: (617) 496-9289. E-mail: holm@chemisty.harvard.edu.

[1] Abbreviations (see also Figure 4): CODH, carbon monoxide dehydrogenase; DMSOR, dimethylsulfoxide reductase; FDH, formate dehydrogenase; FeMoco, iron−molybdenum cofactor; FTIR, Fourier transform infrared; Im, imidazole; L, ligand (generalized); M, metal (generalized); Me_3tacn, *N*,*N*′,*N*″-trimethyl-1,4,7-triazacyclononane; NiR, nitrate reductase; PDB, Protein Data Bank; Q, oxygen, sulfur, or selenium; S_2-*o*-xyl, *o*-xylyl-α,α′-dithiolate(2-); S_2pd, pyranopterindithiolate(3-); SO, sulfite oxidase; XOR, xanthine oxidoreductase.

10.1021/bi900044e CCC: $40.75
Published on Web 02/10/2009

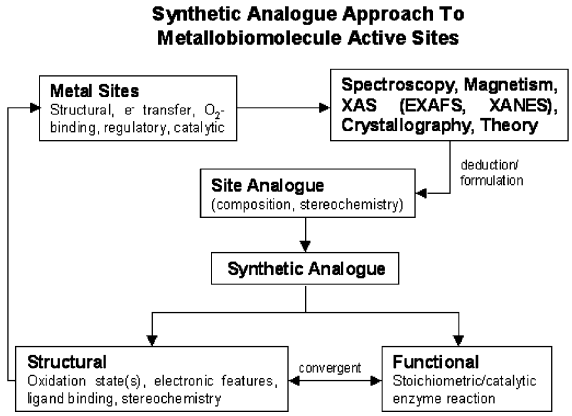

FIGURE 1: Schematic representation of the synthetic analogue approach to metallobiomolecule active sites. The arrow on the left signifies repetition of the process leading to an improved analogue.

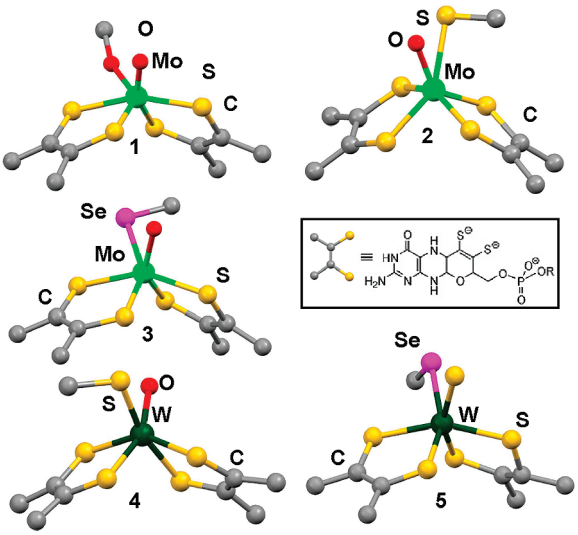

FIGURE 2: Oxidized active site structures in the molybdoenzyme DMSOR family: **1**, DMSO reductase (*Rhodobacter sphaeroides*, 1.3 Å resolution, PDB entry 1EU1, one conformation) (*8*); **2**, dissimilatory nitrate reductase (*Desulfovibrio desulfuricans*, 1.9 Å resolution, PDB entry 2NAP) (*9*); and **3**, formate dehydrogenase N (*Escherichia coli*, 1.6 Å resolution, PDB entry 1KQF) (*10*). Tungsten enzymes: **4**, acetylene hydratase (*Pelobacter acetylenicus*, 1.26 Å resolution, PDB entry 2E7Z) (*12*); and **5**, formate dehydrogenase (*Desulfovibrio gigas*, 1.8 Å resolution, PDB entry 1H0H) (*13*). The pyranopterindithiolate cofactor ligand is depicted in the box (R = nucleotide).

contain two pyranopterindithiolate(3-) cofactor ligands as in distorted trigonal prismatic $\{Mo^{VI}O(L)(S_2pd)_2\}$, where L is O_{Ser} (**1**, DMSOR) (*8*), S_{Cys} (**2**, dissimilatory NiR) (*9*), and Se_{Cys} (**3**, FDH) (*10, 11*). Although FDH catalyzes the $HCO_2^- \leftrightarrow CO_2 + H^+ + 2e^-$ process and not reaction 1, it is placed in the DMSOR family because of site structural similarity. Also shown are the tungstoenzyme sites $\{W^{IV}(OH_2)(S_{Cys})(S_2pd)_2\}$ of acetylene hydratase (**4**) (*12*) and $\{W^{VI}(SH)(Se_{Cys})(S_2pd)_2\}$ of FDH (**5**) (*13*). Sites in the SO and XOR families contain one cofactor ligand (Figure 3) and include the oxidized sites $\{MoO_2(S_{Cys})(S_2pd)\}$ of chicken liver and plant SO (**6**) (*14, 15*), $\{MoO_2S(S_2pd)\}$ of quinoline 2-oxidoreductase (**7**) (*16*), and a substrate complex of the milk XOR site (**8**) (*17*). The wealth of structural information from crystallography and X-ray absorption spectroscopy is the single most important factor leading to the development of active site analogues. The cofactor ligand functions in the ene-1,2-

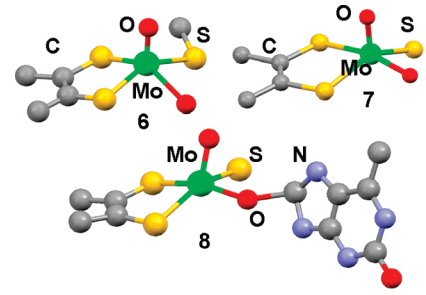

FIGURE 3: Oxidized active site structures in the molybdoenzyme SO and XOR families: **6**, sulfite oxidase (chicken liver, 1.9 Å, PDB entry 1SOX) (*14*); **7**, quinoline-2-oxidoreductase (*Pseudomonas putida*, 1.8 Å resolution, PDB entry 1T3Q) (*16*); and **8**, reaction intermediate of xanthine oxidoreductase and 2-hydroxy-6-methylpurine (2.3 Å, PDB entry 3B9J) (*17*).

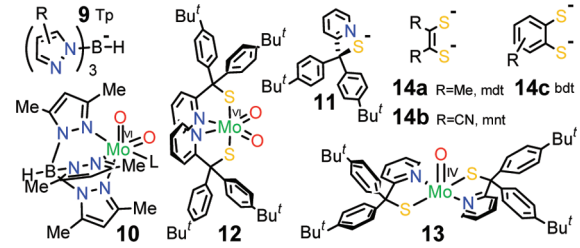

FIGURE 4: Ligands and complexes in biomimetic molybdenum/tungsten chemistry: tridentate hydrotris(pyrazolyl)borate(1-) **9** and an $Mo^{VI}O_2$ complex **10** (L variable), bidentate 2-pyridyldiphenylmethanethiolate(1-) (**11**) and its sterically encumbered $Mo^{VI}O_2$ (**12**) and $Mo^{IV}O$ (**13**) complexes, and dithiolate ligands **14**.

dithiolate form (Figure 2), the terminal reduced member of the dithiolene class of prototypical noninnocent ligands that encompasses oxidation states $(R_2C_2S_2)^{2-}$, $(R_2C_2S_2)^-$, and $(R_2C_2S_2)^0$ (*18*). Biomimetic research focuses on the chemistry of mononuclear complexes in physiological oxidation states M^{IV}, M^V, and M^{VI}.

Of the many non-dithiolene ligand platforms employed, several have proven to be especially useful (Figure 4). Complexes of tridentate hydrotris(pyrazolyl)borate **9** with variable substituents (R) have been valuable in disclosing fundamental properties of molybdenum and tungsten in physiological oxidation states (*19, 20*), albeit not in coordination environments closely similar to enzyme sites. As examples, species such as **10** execute the minimal oxygen atom transfer reaction 2 with disclosure of mechanistic details (*21*) and support proton-coupled electron transfer reactions and a catalytic cycle (*22*) that parallels the enzymatic cycle; another variant sustains the uncommon *cis*-$Mo^{VI}OS$ fragment (*23*) found in the XOR family.

$$Mo^{IV}O + XO \leftrightarrow Mo^{VI}O_2 + X \qquad (2)$$

Bidentate ligand **11** illustrates the concept of steric suppression of nonphysiological reaction 3, allowing reaction 2 with components **12** and **13** and a wide variety of substrates to proceed without complication (*24*).

$$Mo^{IV}O + Mo^{VI}O_2 \leftrightarrow OMo^{V}{-}O{-}Mo^{V}O \qquad (3)$$

Dithiolate ligands **14** closely simulate the structural and electronic features imposed by the cofactor ligand. Three common and useful types are shown, of which **14a** is most like the natural ligand. Substituent variation alters electron density at the sulfur atoms and modulates redox potentials.

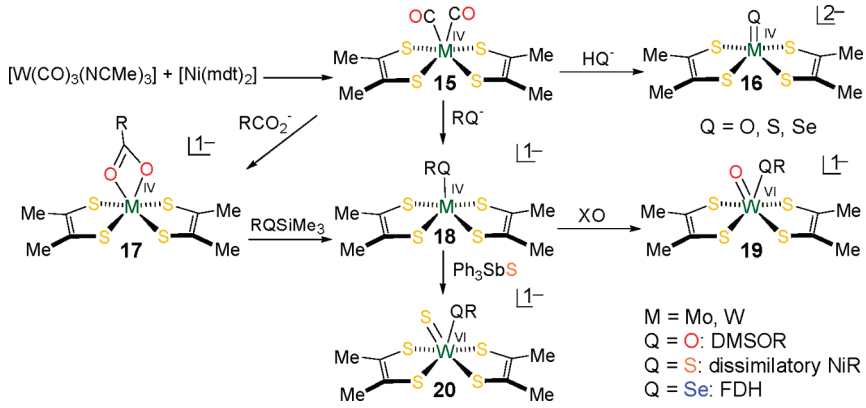

FIGURE 5: Synthesis of unprotonated analogues of reduced (**17** and **18**) and oxidized (**19**) active sites of three members of the DMSOR family (M = Mo; Q = O, S, or Se). Complex **20** is an analogue of the oxidized site in W-FDH. Reduced analogues have square pyramidal structures, and oxidized analogues and **17** adopt six-coordinate structures distorted toward trigonal prismatic geometry.

Structural Analogues. Efficient syntheses afford analogues of reduced (desoxo Mo^{IV}) and oxidized (monooxo Mo^{VI}) sites in the DMSOR family (Figure 5) (*20, 25*−*28*). The mdt ligand has not been isolated as a stable salt but is accessible by the indicated ligand transfer reaction to form M = Mo/W dicarbonyl complexes **15**. The labile carbonyl groups are displaced to yield terminal oxo/sulfido complexes **16**, η^2-carboxylates **17**, and square pyramidal species **18**, which can also be obtained from **17** with silylthio or silylseleno reagents. To ensure stable mononuclear structures, complexes **18** are prepared with sterically bulky R substituents. The scheme is completed by oxo transfer reactions where XO is Me_3NO or Ph_3AsO to give monooxo complexes **19** and by a sulfur atom transfer reaction to afford **20**. These complexes can be isolated only with tungsten. As is the case here, Mo^{VI} complexes are often unstable to autoreduction in anionic sulfur ligand environments. Because isoligated complexes of Mo^{VI}/W^{VI} are always isostructural and practically isometric, the approach has afforded structural analogues **19** of three oxidized sites in the DMSOR family and one analogue **20** of a tungstoenzyme site (compare Figure 2). Further, complexes **18** are analogues of reduced sites; **17** (M = Mo) is a representative of the site of a membrane-bound NiR of *E. coli* (*29*), and Mo=S complex **16** models the formate-reduced site in a reinterpretation of the mechanism of *E. coli* FDH_H (*30*). Analogue complexes are unprotonated versions with an M=Q group rather than the M−QH groups often found in enzyme sites.

Structural analogues of oxidized sites of the SO and XOR families have been synthesized utilizing dithiolate **14c** (Figure 6). A sequence of substitution reactions yields **21**, an analogue of the SO site in which a hindered thiolate simulates the conserved cysteinate in site **6** (*31*). In seeking XOR site analogues, W^{VI} complexes have again been used because of the redox instability of Mo^{VI}. Removal of oxo ligands as siloxane from tungstate precursors leads to **22**, an analogue of an oxidized inactive site, and **23**, an analogue of the site in oxidized active enzymes (*32*). Native sites are often protonated, a condition simulated for structural purposes by silylation to give **24** and **25**. Protonated species have not yet been isolated. Complex **23** is a long-sought structural analogue with a single basal sulfido ligand, as in native site **7**, a position maintained upon reduction by substrate to the (probable) Mo^{IV} state in **8**.

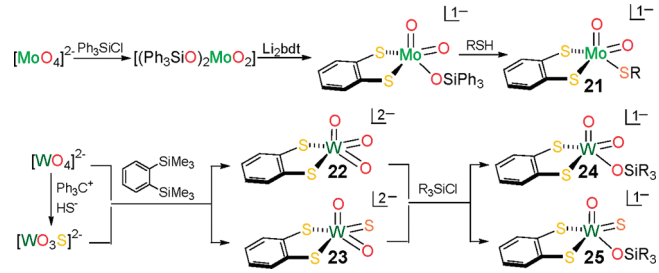

FIGURE 6: Synthetic schemes leading to structural analogues of the active sites of members of the SO (**21**) and XOR (**23**) families. Complex **22** represents an inactive site, and **24** and **25** represent monoprotonated inactive and active sites, respectively, in the XOR family.

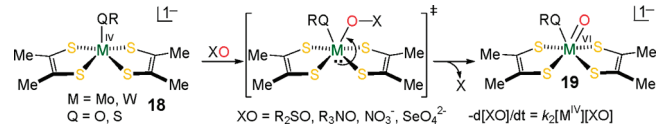

FIGURE 7: Schematic representation of functional reductase analogue reaction systems for *S*-oxides, *N*-oxides, nitrate, and selenate.

Accurate analogues present structures unmodified by a protein environment. Superposition of analogue (**19** and **21**−**25**) and oxidized protein site structures reveals near congruency in most cases, with weighted root-mean-square deviations (rmsd's) in atom positions of ≤0.30 Å (*31*−*33*). Protein interactions evidently do not cause major perturbations of intrinsic structures as represented by analogue complexes in their crystal lattices.

Functional Analogues. Certain of the preceding complexes manifest reductase activity with biological substrates (Figure 7). Complexes **18** cleanly reduce substrate in atom transfer reactions analogous to those of DMSOR and trimethylamine *N*-oxide, nitrate, and selenate reductases (*20, 27, 28*), albeit at much slower rates. The $Mo^{VI}O$ analogues **19** were generated as reaction products but not isolated. Reactions are second-order with associative transition states; activation parameters for the reduction of $(CH_2)_4SO$ by $[Mo(OPh)(mdt)_2]^-$ in acetonitrile (k_2^{298} = 1.5 × 10^4 M^{-1} s^{-1}) are typical: $\Delta H^{\ddagger}$ = 10 kcal/mol, and $\Delta S^{\ddagger}$ = −39 eu. These reactions exhibit a small kinetic metal effect ($k_2^W/k_2^{Mo} \approx$ 6−30) in the reduction of a constant substrate. A related effect observed with molybdenum and tungsten isoenzymes is intrinsic to the metals and is associated with the periodic behavior of isostructural and isoelectronic redox couples of the two metals. These reactions simulate the oxo atom

transfer step in a single turnover of an enzyme. In a functional NiR analogue system, oxo transfer reaction 5 is coupled to equilibrium reaction 4 in dichloromethane with the result that Michaelis−Menten saturation kinetics are followed (*34*).

$$[Mo^{IV}(SR)(PPh_3)(mnt)_2]^{2-} \leftrightarrow [Mo^{IV}(SR)(mnt)_2]^{2-} + PPh_3 \quad (4)$$

$$[Mo^{IV}(SR)(mnt)_2]^{1-} + NO_3^- \rightarrow [Mo^{VI}O(SR)(mnt)_2]^{1-} + NO_2^- \quad (5)$$

Molybdenum and tungsten dithiolene complexes form the basis for systems in which both accurate structural and suitably functional analogues have been realized, an ultimate but infrequently achieved goal in synthetic analogue chemistry. Functional analogues refer to oxotransferases that are reductases. However, the picture will remain incomplete pending the development of oxidase analogue systems. One such system has been briefly described in relation to arsenite oxidase (*35*). As yet, there are no effective systems for substrates of the XOR family. These enzymes are hydroxylases that utilize Mo^{VI}−OH units as base-activated nucleophiles in the reaction pathway rather than metal sites as oxygen atom donors or acceptors (*6*).

HYDROGENASES

Hydrogenases occur in bacteria, archaea, and eukarya and catalyze bidirectional reaction 6.

$$H_2 \leftrightarrow 2H^+ + 2e^- \quad (6)$$

They consist of two main classes, the [NiFe] (*36, 37*) and [FeSe] (*37*−*39*) hydrogenases, so designated because of their active site metal content. A subgroup of the first class consists of the [NiFeSe] hydrogenases which contain a selenocysteinate in place of a cysteinate ligand. Members of a third class, [Fe] hydrogenases, contain mononuclear sites (*40*) and are not considered here. Synthetic approaches to [NiFe] and [FeFe] enzyme sites require construction of binuclear species and, in the latter case, attachment to an Fe_4S_4 cubane-type cluster. The binuclear site and site fragment structures project an apparent attainability, which together with the importance of the problem, has resulted in extensive activity in site modeling, many aspects of which have been summarized (*41*−*45*). We truncate the subject to a small set of attractive developments.

[NiFe] Hydrogenases. A combination of X-ray crystallographic and FTIR studies has led to the formulations **26a** for the oxidized site and **27a** for the reduced site (Figure 8) (*36, 37, 46, 47*). For each, a specific structure **26b** (*48*) or **27b** (*49*) is provided. In the oxidized site, X is a generalized bridging ligand, thought to be an oxygenic species as indicated by O in **26b**, while in the reduced site, the bridging position is vacant or perhaps occupied by hydride. Appropriate initial analogues are heterometal binuclear species containing the $(RS)_2Ni^{II}(\mu_2\text{-}SR)_2Fe^{II}$ fragment with Ni−Fe separations of 2.5−2.9 Å and distorted octahedral low-spin Fe^{II} coordinated to one carbonyl and two cyanide ligands. A significant portion of synthetic research has focused on mononuclear iron or nickel sites (Figure 9). Among sulfur-ligated species, **28** reproduces $Fe(CN)_2(CO)$

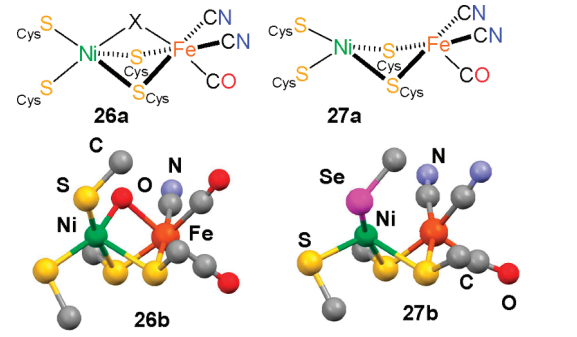

FIGURE 8: Representative hydrogenase active site structures: oxidized [NiFe] (**26a**) and a specific example (**26b**, *Desulfovibrio vulgaris*, 1.4 Å resolution, PDB entry 1WUJ) (*48*) and reduced [NiFe] (**27a**) and a specific example of reduced [NiFeSe] (**27b**, *Desulfovibrio maculatum*, 2.15 Å resolution, PDB entry 1CC1) (*49*).

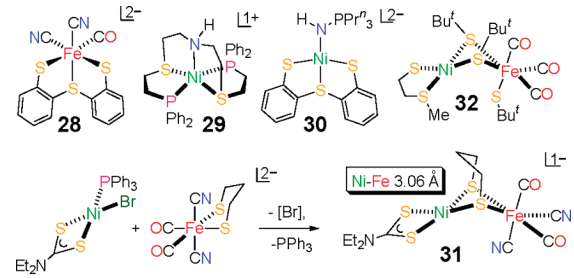

FIGURE 9: Mononuclear complexes **28**−**30** and NiFe complex **32**, and preparation of NiFe complex **31**.

coordination at the low-spin Fe^{II} site (*50*), **29** evolves dihydrogen from HCl nearly quantitatively in the overall reaction $Ni^I + H^+ \rightarrow Ni^{II} + {}^1/_2H_2$ (*51*), and **30** catalyzes D_2−H^+ exchange consistent with enzymatic heterolytic cleavage of D_2 or H_2 (*52*). A variety of dinuclear Ni−Fe complexes can be accessed by reactions of suitable mononuclear components, as in the formation of **31** (*53*). This molecule illustrates the feasibility of the $Ni^{II}(\mu_2\text{-}SR)_2Fe^{II}$ bridge fragment, low-spin Fe^{II} in the unit $Fe(SR)_2(CN)_2(CO)_2$, and a Ni···Fe separation near the upper end found in enzyme sites. Complex **32** reveals stabilization of low-spin Fe^{II} in a site containing three strong field ligands and contains a similar bridge fragment with exclusive sulfur coordination at Ni^{II} but a considerably longer Ni···Fe distance (3.29 Å) (*54*). No functional dinuclear Ni−Fe analogues have yet been devised. However, in a variation on a native metal, the $Fe^{II}(CN)_2(CO)$ unit was replaced by isoelectronic $(C_6Me_6)Ru^{II}$ to give a complex with the bridge $Ni^{II}(\mu_2\text{-}SR)_2Ru^{II}$ incorporating a metal that forms stable dihydrogen complexes. The complex reacts with dihydrogen in water, affording a structurally related dinuclear product augmented with the $Ni^{II}(\mu_2\text{-}H)Ru^{II}$ hydride bridge and protons released in solution (*55*). A plausible intermediate in the enzymatic uptake of H_2 is site **27a** with hydride occupying the vacant bridge position.

[FeFe] Hydrogenases. The active sites of these enzymes are termed H-clusters and exist in three oxidation levels, air-oxidized inactive ($Fe^{II}Fe^{II}$), oxidized active ($Fe^{II}Fe^{I}$), and reduced active ($Fe^{I}Fe^{I}$), with the proposed oxidation states indicated. The structure of an oxidized active site **33** (Figure 10) (*56*) reveals a dinuclear $Fe_2(\mu_2\text{-}CO)(\mu_2\text{-}SR)_2(CO)_2(CN)_2$ fragment containing the dithiolate SCH_2XCH_2S (in which atom or group X is CH_2, NH, or O and is not definitely identified) linked by an $Fe(\mu_2\text{-}S_{Cys})Fe$ bridge to an Fe_4S_4 cluster. The iron sites are

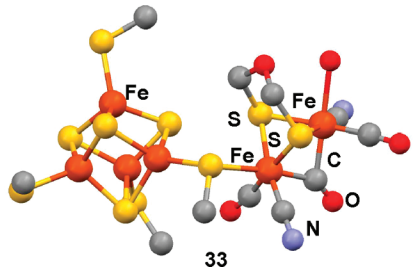

FIGURE 10: Structure of the H-cluster of an [FeFe] hydrogenase in the oxidized active form (**33**, *Clostridium pasteurianum*, 1.4 Å resolution, PDB entry 3C8Y) (*56*). In the dinuclear fragment, the carbonyl bridge is slightly asymmetric (Fe−C, 1.91 and 1.96 Å) and the Fe−Fe distance (2.55 Å) is consistent with direct metal−metal interaction.

six-coordinate, and that distal to the cysteinate bridge contains an aquo ligand. The problem reduces to synthesis of a suitable dinuclear fragment and attachment through an unsupported bridge to the Fe_4S_4 cluster.

Approaches to the dinuclear fragment often begin with the Seyferth anion, $[Fe^{I}_2S_2(CO)_6]^{2-}$, which is readily dialkylated to $[Fe_2(SR)_2(CO)_6]$ (*57*), thereby generating a core structure closely related to that in **33**. Structures with variable X and substitution of cyanide or tertiary phosphine for carbonyl have been achieved in extensive modeling studies (*41, 43*). Carbon monoxide, cyanide, and phosphine have the common properties of π-acid behavior and stabilization of low oxidation states. In one example of structural modeling (Figure 11), dithiolate cluster **34** undergoes CO substitution to place the phosphines in **35** at the positions of cyanide in **33**, followed by oxidation to yield $Fe^{II}Fe^{I}$ product **36** with an asymmetric carbonyl bridge (*58*). An approach to the entire H-cluster framework is represented by the reaction of 1:3 subsite-differentiated cluster **37** (*59*) with functionalized **38** to afford a product whose physicochemical properties have been interpreted in terms of the assembly **39** in which the cluster and dinuclear unit are linked by an unsupported Fe(μ_2-SR)Fe bridge (*60*). The viability of the structure is supported by DFT calculations which indicate the $Fe^{I}Fe^{I}$ and $[Fe_4S_4]^{2+}$ oxidation levels. The H-cluster model and certain dinuclear species are catalysts for electrochemical dihydrogen evolution at strongly reducing potentials (*61*), while another $Fe^{I}Fe^{I}$ complex activates dihydrogen photochemically in the form of an $Fe^{II}Fe^{II}$ dihydride (*62*).

IRON−SULFUR PROTEINS

These proteins are of widespread occurrence at all levels of life and are implicated in electron transfer and other multifarious functions (*63, 64*). Clusters with rhomboidal Fe_2S_2 (**40** and **41**) (*65, 66*), cuboidal Fe_3S_4 (**42**) (*67*), and cubane-type Fe_4S_4 (**43**) (*68*) cores (Figure 12) are ubiquitous and exist in at least two oxidation states necessary for redox behavior. Analogues of **40**, **43**, and the $\{Fe(S_{Cys})_4\}$ site in rubredoxins (not shown) were prepared at the very beginning of biomimetic inorganic chemistry and were followed later by an analogue of **42**. Different core oxidation states are achieved by appropriate choice of Fe^{II} or Fe^{III} reactants in synthesis or by redox reactions of isolated clusters. The development and accomplishments of iron−sulfur analogue chemistry and a summary of synthetic methods affording iron−sulfur clusters are available (*69, 70*). In analogue clusters, terminal cysteinate ligation is a simulated by organic thiolates. Despite the advanced state of iron−sulfur analogue chemistry, several problems, including the complicated clusters of nitrogenase and carbon monoxide dehydrogenase (vide infra), remain, while progress has been made on two others, the Rieske cluster and the fully reduced Fe_4S_4 cluster of the Fe protein of nitrogenase.

Rieske proteins function in electron transport and contain cluster **41**, differentiated from the more common Fe_2S_2 cluster **40** by the presence of two Im_{His} ligands (*71*). Reaction of $[Fe_2S_2Cl_4]^{2-}$ with *o*-xylyldithiolate and the dilithium salt of 2,2′-bis(methylindolyl)phenylmethane affords $Fe^{III}Fe^{III}$ complex **44** (Figure 13), having the same ligation pattern as **41** (*72*). It undergoes a reversible one-electron reduction at a potential ~150 mV less negative than that of $[Fe_2S_2(S_2\text{-}o\text{-xyl})_2]^{2-}$, an accurate analogue of **40**, and exhibits a rhombic EPR spectrum similar to that of a reduced ($Fe^{III}Fe^{II}$) Rieske center. Potentials of proteins with cluster **40** are more negative than those of Rieske proteins, which encompass the range from −150 to 400 mV versus the standard hydrogen electrode, a variability largely due to electrostatic effects (*73*). Reduction of **44** apparently occurs at the FeN_2S_2 site, as for Rieske centers. Although this cluster is not an exact analogue of a Rieske cluster because of binding of two anionic nitrogen ligands rather than neutral imidazoles, it is the closest approach yet to the native cluster itself.

Cubane-type clusters **43** are the most widely dispersed of all iron−sulfur species and are well-known in proteins and analogue molecules in electronically delocalized core oxidation states 3+, 2+, and 1+ of redox series 7, in which adjacent members are interconverted by one-electron transfer.

$$\underset{4Fe^{2+}}{[Fe_4S_4]^{0}} \leftrightarrow \underset{3Fe^{2+}+Fe^{3+}}{[Fe_4S_4]^{+}} \leftrightarrow \underset{2Fe^{2+}+2Fe^{3+}}{[Fe_4S_4]^{2+}} \leftrightarrow \underset{Fe^{2+}+3Fe^{3+}}{[Fe_4S_4]^{3+}} \qquad (7)$$

The proposal that the Fe protein of nitrogenase might utilize the $[Fe_4S_4]^{2+/+}$ and $[Fe_4S_4]^{+/0}$ couples in delivering electrons to the catalytic site of nitrogenase was followed by definite proof of the existence of the $[Fe_4S_4]^{0}$ oxidation state in the fully reduced Fe protein (*74, 75*). These results render an isolable all-ferrous analogue a significant objective. The first such species was isolated from the substitution reaction of $[Fe_4S_4(PPr^{i}_3)_4]^{+}$ with cyanide in the presence of the strong reductant $[Ph_2CO]^{\bullet-}$ (*76*). However, $[Fe_4S_4(CN)_4]^{4-}$, while in the desired oxidation state, was intensely unstable to oxidation and difficult to manipulate. Use of an N-heterocyclic carbene as a strong σ-donor terminal ligand in a cluster assembly system with an Fe^{II} reactant and a soluble sulfide source leads to cluster **45** (Figure 13) (*77*), which is amenable to study. Its ^{57}Fe isomer shift and comparative structural parameters are fully consistent with an all-ferrous formulation. Further, the magnetic Mössbauer and integer spin EPR spectra of **45** disclose the unusual $S = 4$ spin ground state (*78*), also found for the fully reduced native Fe protein (*74*), where it is unique in biology. The synthetic cluster is a meaningful analogue of the protein-bound $[Fe_4S_4]^{0}$ cluster, providing further evidence that magnetic properties arise from interactions within the core and are not strongly influenced by terminal ligation (here S_{Cys} vs $C_{carbene}$). The two all-ferrous clusters complete the synthesis of isolable analogues of all known biological oxidation states of Fe_4S_4 clusters.

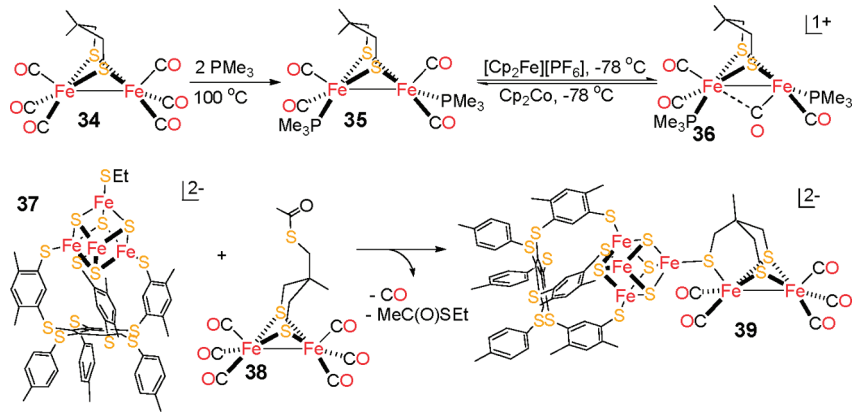

FIGURE 11: Reactions leading to a models of the dinuclear fragment (**36**) and the entire framework (**39**) of the H-cluster.

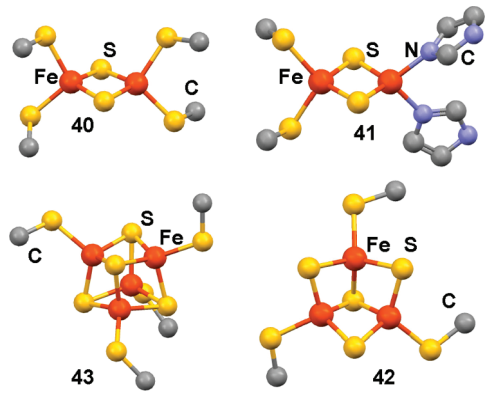

FIGURE 12: Structures of clusters $\{Fe_2S_2(S_{Cys})_4\}$ (**40**, *Anabaena*, 1.2−1.3 Å resolution, PDB entry 1CZP) (*65*), $\{Fe_2S_2(S_{Cys})_2(N_{His})_2\}$ (**41**, *Sulfolobus acidocaldarius*, 1.1 Å resolution, PDB entry 1JM1) (*66*), $\{Fe_3S_4(S_{Cys})_3\}$ (**42**, *Pyrococcus furious*, 1.5 Å resolution, PDB entry 1SJ1) (*67*), and $\{Fe_4S_4(S_{Cys})_4\}$ (**43**, *Bacillus thermoproteolyticus*, 0.9−1.0 Å resolution, PDB entry 1IQZ) (*68*).

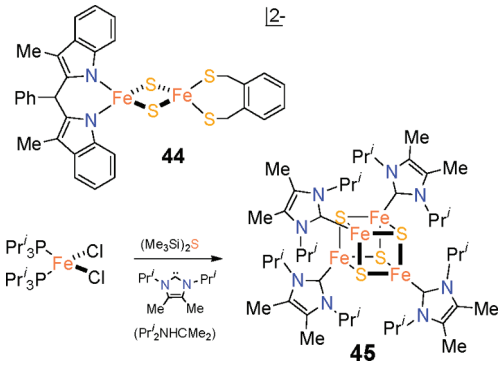

FIGURE 13: Oxidized Rieske cluster analogue **44** and the preparation of all-ferrous analogue **45** of the fully reduced cluster in the Fe protein of nitrogenase.

CARBON MONOXIDE DEHYDROGENASES

These enzymes occur in aerobic and anaerobic bacteria and archaea and catalyze the reversible interconversion of carbon monoxide and carbon dioxide in reaction 8 at two very different types of catalytic sites.

$$CO + H_2O \leftrightarrow CO_2 + 2H^+ + 2e^- \qquad (8)$$

Cu−Mo CODH occurs in aerobic organisms (*79*), while Ni−Fe CODHs are found in anaerobic organisms (*80*−*82*). The enzymes are highly significant agents in global carbon cycling. Synthetic analogue chemistry of their catalytic sites is at an early stage.

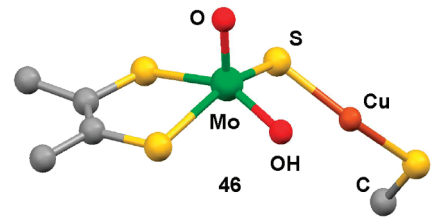

FIGURE 14: Oxidized active site structure of Cu−Mo CODH (**46**, *Oligotropha carboxidovorans*, 1.1 Å resolution, PDB entry 1N5W) (*83*) (Cu···Mo, 3.74 Å; Mo−S, 2.27 Å; Cu−S, 2.21 Å; Cu−S_{Cys}, 2.22 Å; Mo−S−Cu, 113°; S−Cu−S, 156°). The reduced site (Mo^{IV}/Cu^{I}) has the same structure with small differences in parameters except for the Mo−S−Cu angle and the Mo···Cu distance which increase by ∼10° and ∼0.5 Å, respectively.

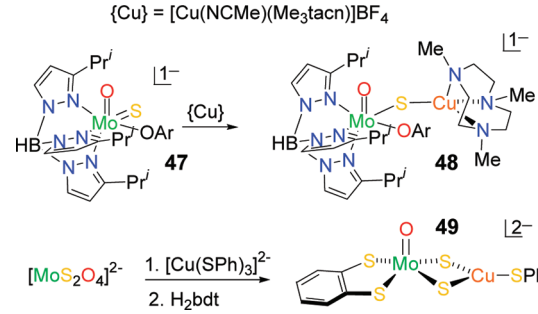

FIGURE 15: Synthetic routes to bridged complexes **48** and **49** having certain structural elements in common with Mo−Cu CODH site **46**.

Mo−Cu CODH. Oxidized site **46** [Mo^{VI}/Cu^{I} (Figure 14)] (*83*) resembles site **7** in the XOR family (Figure 3) with the inclusion of a Cu^{I}−S_{Cys} fragment bound to the basal sulfido ligand. Two synthetic approaches to the site have emerged (Figure 15). Reaction of a Cu^{I} triazamacrocyclic complex with six-coordinate $Mo^{V}OS$ complex **47** results in displacement of acetonitrile and formation of assembly **48** (*84*). This species establishes the synthetic viability of an unsupported Mo^{V}−S−Cu^{I} bridge based on an initially terminal sulfido ligand; metric features (Mo−S, 2.284 Å; Cu−S, 2.135 Å; Mo−S−Cu, 118.9°; Mo···Cu, 3.74 Å) resemble those of site **46**. Further, EPR spectra and DFT calculations establish that unpaired electron density extends to the Cu^{I} site. While this complex lacks dithiolate binding simulating the cofactor ligand, it provides another example of the utility of the hydrotris(pyrazolyl)borate ligand platform in stabilizing a structural element of a molybdoenzyme site. A second relevant reaction affords square pyramidal Mo^{VI} complex **49** that incorporates the enzyme site features of an apical oxo

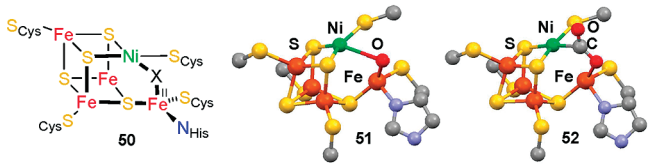

FIGURE 16: Generalized structure **50** of Ni−Fe CODH sites **51** and **52** (*C. hydrogenoformans*, 1.4−1.5 Å resolution, PDB entry 3B52) (*90*).

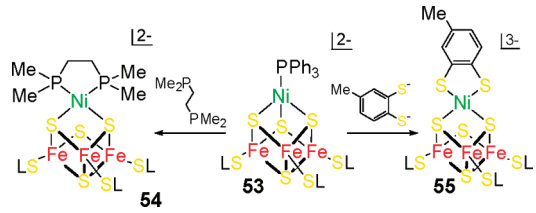

FIGURE 17: Synthesis of cubanoid clusters **54** and **55** by ligand substitution of **53**. The 3 LS notation refers to the tridentate thiolate ligand in cluster **37** (Figure 11).

atom, basal dithiolate coordination, and basal sulfido coordination to Cu^{I} (*85*). However, it departs from **46** with two sulfido ligands which form mutually supported bridges to Cu^{I}. Complexes **23** and **25** (Figure 6) offer the possibility of a single basal sulfido bridge in square pyramidal coordination as in **46** but with a non-native metal. The reactivity of these species with Cu^{I} is currently under investigation in this laboratory.

Ni−Fe CODH. Structures of the catalytic sites, termed C-clusters and depicted generally by **50** which subsumes actual structures **51** and **52** (Figure 16), have the common features of a cubanoid $NiFe_3S_4$ core with an approximately planar nickel site and a tetrahedral Fe^{II} site bridged to the core by atom or group X and a μ_3-S atom. Construction of a site analogue can be proposed in two steps: synthesis of the $NiFe_3S_4$ core containing planar Ni^{II} followed by binding of Fe^{II} to the cluster through the μ_2-S atom axial to Ni^{II} and a Ni−X−Fe bridge. The conversion of previously prepared cubane-type cluster **53** (*86*) to **54** and **55** by substitution with strong-field in-plane ligands involves spin pairing with a concomitant tetrahedral ($S = 1$) → planar ($S = 0$) Ni^{II} structural change and creation of a μ_2-S atom axial to the nickel site (Figure 17) (*87, 88*). This accomplishes the first step. The structure of the C-cluster of CODH from *Carboxydothermus hydrogenoformans* (1.1 Å resolution) was interpreted in terms of an X = S bridge (*89*), prompting the introduction of a dithiolate ligand in **55** which might sustain a sulfur bridge to external Fe^{II}. More recently, the crystal structure of recombinant CODH maintained at fixed redox potentials revealed C-clusters of the same overall structure but with X being OH/OH_2 in **51** and CO_2 in **52** (Figure 16) after treatment with $NaHCO_3$ at a lower potential (*90*). This and other evidence indicate that the bridge in the active enzyme does not contain sulfide. The central feature of a structure-based mechanism involves nucleophilic attack by an Fe^{II}−OH group on the carbon atom in Ni^{II}−CO. The Ni^{II}−OH/OH_2−Fe^{II} bridge unit is unknown in any synthetic species. Consequently, the second step in creating a C-cluster remains a formidable challenge.

NITROGENASE

The nitrogenase complex catalyzes the six-electron reduction reaction 9 with simultaneous dihydrogen evolution and

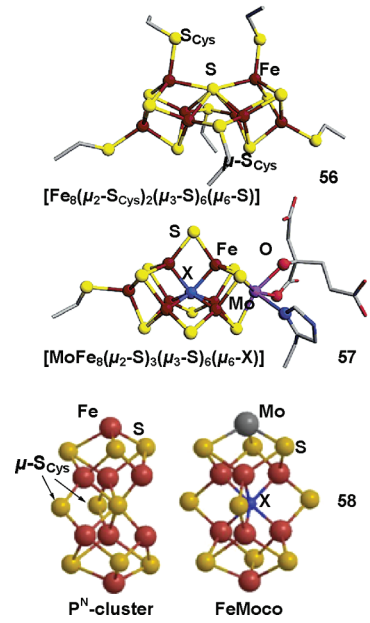

FIGURE 18: Structures of P-cluster **56** and FeMoco **57** (*Azotobacter vinelandii* MoFe protein, 2.0 and 1.2 Å resolution, PDB entries 2MIN and 1M1N, respectively) of nitrogenase (*93, 95*) and a comparison of **58** of cluster topologies.

consists of an α_2-Fe protein with an Fe_4S_4 cluster bound between subunits and an $\alpha_2\beta_2$-MoFe protein containing two clusters in each $\alpha\beta$ subunit (*91, 92*).

$$N_2 + 6H^+ + 6e^- \rightarrow 2NH_3 \qquad (9)$$

The P-cluster is located at the $\alpha\beta$ interface, and the cofactor cluster FeMoco is placed within the α subunit. The path of electron flow is most likely Fe_4S_4 → P-cluster → FeMoco; the substrate is bound and reduced at the cofactor cluster by a pathway yet to be defined. Synthetic attempts directed at the P-cluster (**56**) and FeMoco (**57**) (Figure 18) (*93*−*95*), arguably the two most complicated and synthetically formidable metalloclusters in biology, commenced well before 1992 when the first crystallographic results at atomic resolution became available. The topological relationship between the two clusters is evident from comparison **58**. The P-cluster contains a μ_6-S interior atom within a $Fe_6(\mu_2\text{-}S_{Cys})_2$ cavity and FeMoco an interstitial μ_6-X atom (X = C, N, or O) (*95*) within a $Fe_6(\mu_2\text{-}S)_3$ cage. We describe here certain encouraging developments. More extensive accounts of work in this laboratory are available (*96, 97*).

Biomimetic cluster synthesis is based on three conceptual strategies (*96, 97*): (i) self-assembly, self-organizing synthesis of clusters from simple mononuclear metal precursors and ligand reagents (the cornerstone approach for cluster synthesis); (ii) fragment condensation, coupling of preexisting di- or polynuclear clusters or a cluster with a mononuclear reactant to give higher-nuclearity clusters of (in theory) predictable structures; and (iii) core conversion, reorganization of a preexisting cluster to a different core geometry by means of redox reactions, changes in ligand set, or reaction with an external reagent, usually a ligand nucleophile. All have proven useful in biomimetic research; strategies (i) and (iii) are illustrated below.

Heterometal cubane-type clusters with $[MFe_3S_4]^z$ cores, including those where M is Mo and V, have been prepared

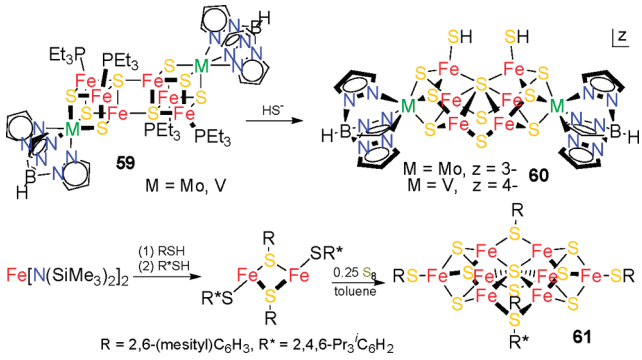

FIGURE 19: Synthetic reactions affording topological analogues of the P-cluster (**60**) and cofactor cluster (**61**) of nitrogenase.

by procedures (i) and (ii) (*97*). A sequence of reactions has been devised on the basis of these single cubane clusters, leading to the all-ferrous edge-bridged double cubanes **59** (Figure 19) (*98*). The clusters, which are attractive precursors because of their high nuclearity, undergo core conversion upon reaction with hydrosulfide in acetonitrile to afford clusters **60** (*99, 100*). These clusters feature a prominent μ_6-S interior atom, have an overall connectivity pattern identical to that of **56**, and map closely upon the native P-cluster with rmsd's in atom positions of 0.33−0.38 Å (*97*). Clusters **60** are first topological analogues of the P-cluster. They are not chemical models because of the presence of heterometals and μ_2-S rather than thiolate bridges. Earlier, the same topology had been achieved in larger and less tractable clusters in which P-type units were connected by sulfide bridges (*101, 102*).

An exceptional result has been obtained by cluster self-assembly in a system containing an Fe^{II} precursor with strongly basic ligands, two thiols which when deprotonated function as exceptionally capacious ligands, and elemental sulfur in toluene (Figure 19) (*103*). Product cluster **61** (28% yield) was isolated; it was also obtained in an assembly system not requiring prior isolation of the dinuclear intermediate. A second cluster with $(Me_3Si)_2N^-$ in a doubly bridging position was formed in a small amount. The toluene solvent promotes the formation of a neutral cluster in a redox-buffered reaction system containing oxidant (sulfur) and reductants (Fe^{II}, thiolate) which generates a product with $5Fe^{II} + 3Fe^{III}$. Remarkably, **61** manifests the FeMoco topology but with μ_2-SR/R* bridges rather than sulfide and sulfide rather than X as the interstitial atom. In addition to achieving the desired topology, the results demonstrate for the first time the formation of an iron−sulfur cluster with an atom interstitial to a trigonal prismatic Fe_6 cage. Taken together, clusters **60** and **61** and the methods affording them presage continued progress toward the goal of accurate synthetic analogues of the P-cluster and FeMoco.

PROSPECTS

A perspective on biomimetic research of metallosites as presented here is offered by an earlier commentary from this laboratory (*96*). "Traditionally, synthetic inorganic chemistry has provided the molecular intuition needed to interpret metal behavior in biological systems. Today, in a reversal of circumstance, metallobiomolecules are posing fundamental inorganic questions whose answers lie outside our existing knowledge. It is a fitting symmetry that the relationship between inorganic chemistry and biology has come full circle. Equally important, these [synthetic] efforts have also contributed broadly to basic areas of inorganic chemistry that would probably not have been examined otherwise; the intrinsic value of such exploration should not be underestimated." Given the progress thus far and the growing sophistication of biomimetic methodologies, it may be anticipated that the unachieved structural analogues of the polynuclear sites set out here will be realized. The value of analogues as structural guides or determinants (Figure 1) is diminishing as the power and productivity of crystallography and spectroscopic methods flourish.

Two additional aspects of research in this field continue apace. One is the daunting challenge of analogue systems capable of enzymatic transformations using chemical apparatus as faithful to native catalysts as possible. While an operative pathway can be won only from an enzyme itself, interrogation of analogue systems can show what is possible, among which may be the actual mechanism. It remains to be learned whether diverse functional analogues operative outside of a protein and suitable for disclosure of mechanistic information can be created. Another aspect is synthesis. While experimental protocol may not be the same, the intent differs not at all from the total synthesis of organic natural products and its contribution to biosynthetic pathways. Such work not only is intended to reach targets but also may contribute to the broad and developing area of biosynthesis of metallocenters (*104*) by showing what synthetic routes are feasible in the absence, and possibly in the presence, of proteins. Problems in metallocenter assembly, whether in vivo or by chemical synthesis, are at the forefront of contemporary metallobiochemistry. One need look no further than the current state of understanding of the biosynthetic pathway of FeMoco (*105, 106*) for an inspiring example.

REFERENCES

1. Holm, R. H., and Solomon, E. I. (2004) Preface: Biomimetic Inorganic Chemistry. *Chem. Rev. 104*, 347–348.
2. Holm, R. H., and Solomon, E. I., Eds. (2004) Biomimetic Inorganic Chemistry. *Chemical Reviews*, Vol. 104, Issue 2, American Chemical Society, Washington, DC.
3. Kraatz, H.-B., and Metzler-Nolte, N., Eds. (2006) *Concepts and Models in Bioinorganic Chemistry*, Wiley-VCH, New York.
4. Hille, R. (1996) The Mononuclear Molybdenum Enzymes. *Chem. Rev. 96*, 2757–2816.
5. Schindelin, H., Kisker, C., and Rajagopalan, K. V. (2001) Molybdopterin from Molybdenum and Tungsten Enzymes. *Adv. Protein Chem. 58*, 47–94.
6. Hille, R. (2006) Structure and Function of Xanthine Oxidoreductase. *Eur. J. Inorg. Chem.*, 1913–1926.
7. Schwarz, G., and Mendel, R. R. (2006) Molybdenum Cofactor Biosynthesis and Molybdenum Enzymes. *Annu. Rev. Plant Biol. 57*, 623–647.
8. Li, H.-K., Temple, C., Rajagopalan, K. V., and Schindelin, H. (2000) The 1.3 Å Crystal Structure of *Rhodobacter sphaeroides* Dimethylsulfoxide Reductase Reveals Two Distinct Molybdenum Coordination Environments. *J. Am. Chem. Soc. 122*, 7673–7680.
9. Dias, J. M., Than, M. E., Humm, A., Huber, R., Bourenkov, G. P., Bartunik, H. D., Bursakov, S., Calvete, J., Caldeira, J., Carneiro, C., Moura, J. J. G., Moura, I., and Romão, M. J. (1999) Crystal Structure of the First Dissimilatory Nitrate Reductase at 1.9 Å Solved by MAD Methods. *Structure 7*, 65–79.
10. Jormakka, M., Törnroth, S., Byrne, B., and Iwata, S. (2002) Molecular Basis of Proton Motive Force Generation: Structure of Formate Dehydrogenase-N. *Science 295*, 1863–1868.
11. Boyington, J. C., Gladyshev, V. N., Khangulov, S. V., Stadtman, T. C., and Sun, P. D. (1997) Crystal Structure of Formate

Dehydrogenase H: Catalysis Involving Mo, Molybdopterin, Selenocysteine, and an Fe_4S_4 Cluster. *Science 275*, 1305–1308.
12. Seiffert, G., Ullman, G. M., Messerschmidt, A., Schinck, B., Kroneck, P. H. M., and Einsle, O. (2007) Structure of the Non-redox-active Tungsten/[4Fe:4S] Enzyme Acetylene Hydratase. *Proc. Natl. Acad. Sci. U.S.A. 104*, 3073–3077.
13. Raaijmakers, H., Macieira, S., Dias, J. M., Texeira, S., Bursakov, S., Huber, R., Moura, J. J. G., Moura, I., and Romão, M. J. (2002) Gene Sequence and the 1.8 Å Crystal Structure of the Tungsten-Containing Formate Dehydrogenase from *Desulfovibrio gigas*. *Structure 10*, 1261–1272.
14. Kisker, C., Schindelin, H., Pacheco, A., Wehbi, W. A., Garrett, R. M., Rajagopalan, K. V., Enemark, J. H., and Rees, D. C. (1997) Molecular Basis of Sulfite Oxidase Deficiency from the Structure of Sulfite Oxidase. *Cell 91*, 973–983.
15. Schrader, N., Fischer, K., Theis, K., Mendel, R. R., Schwarz, G., and Kisker, C. (2003) The Crystal Structure of Plant Sulfite Oxidase Provides Insights into Sulfite Oxidation in Plants and Animals. *Structure 11*, 1251–1263.
16. Bonin, I., Martins, B. M., Purvanov, V., Fetzner, S., Huber, R., and Dobbek, H. (2004) Active Site Geometry and Substrate Recognition of the Molybdenum Hydroxylase Quinoline 2-Oxidoreductase. *Structure 12*, 1425–1435.
17. Pauff, J. M., Zhang, J., Bell, C. E., and Hille, R. (2008) Crystal Structure of Enzyme in Reaction with 2-Hydroxy-6-methylpurine. *J. Biol. Chem. 283*, 4818–4824.
18. Kirk, M. L., McNaughton, R. L., and Helton, M. E. (2004) The Electronic Structure and Spectroscopy of Metallo-Dithiolene Complexes. *Prog. Inorg. Chem. 52*, 111–212.
19. Young, C. G. (2000) in *Biomimetic Oxidations Catalyzed by Transition Metal Complexes* (Meunier, B., Ed.) pp 415−459, World Scientific Publishing Co., Singapore.
20. Enemark, J. H., Cooney, J. J. A., Wang, J.-J., and Holm, R. H. (2004) Synthetic Analogues and Reaction Systems Relevant to the Molybdenum and Tungsten Oxotransferases. *Chem. Rev. 104*, 1175–1200.
21. Kail, B. W., Pérez, L. M., Zaric, S. D., Millar, A. J., Young, C. G., Hall, M. B., and Basu, P. (2006) Mechanistic Investigation of the Oxygen-Atom-Transfer Reactivity of Dioxo-molybdenum(VI) Complexes. *Chem.—Eur. J. 12*, 7501–7509.
22. Xiao, Z., Bruck, M. A., Enemark, J. H., Young, C. G., and Wedd, A. G. (1996) A Catalytic Cycle Related to Molybdenum Enzymes Containing $[Mo^{VI}O_2]^{2+}$ Oxidized Active Sites. *Inorg. Chem. 35*, 7508–7515.
23. Doonan, C. J., Rubie, N. D., Peariso, K., Harris, H. H., Knottenbelt, S. Z., George, G. N., Young, C. G., and Kirk, M. L. (2008) Electronic Description of the *cis*-MoOS Unit in Models for Molybdenum Hydroxylases. *J. Am. Chem. Soc. 130*, 55–65.
24. Schultz, B. E., Gheller, S. F., Muetterties, M. C., Scott, M. J., and Holm, R. H. (1993) Molybdenum-Mediated Oxygen Atom Transfer: An Improved Analogue Reaction System of the Molybdenum Oxotransferases. *J. Am. Chem. Soc. 115*, 2714–2722.
25. Jiang, J., and Holm, R. H. (2004) An Expanded Set of Functional Groups in Bis(dithiolene)tungsten(IV,VI) Complexes Related to the Active Sites of Tungstoenzymes, Including W^{IV}-SR and W^{VI}-O(SR). *Inorg. Chem. 43*, 1302–1310.
26. Wang, J.-J., Kryatova, O., Rybak-Akimova, E. V., and Holm, R. H. (2004) Comparative Kinetics and Mechanism of Oxygen and Sulfur Atom Transfer Reactions Mediated by Bis(dithiolene) Complexes of Molybdenum and Tungsten. *Inorg. Chem. 43*, 8092–8101.
27. Jiang, J., and Holm, R. H. (2005) Reaction Systems Related to Dissimilatory Nitrate Reductase: Nitrate Reduction Mediated by Bis(dithiolene)tungsten Complexes. *Inorg. Chem. 44*, 1068–1072.
28. Wang, J.-J., Tessier, C., and Holm, R. H. (2006) Analogue Reaction Systems of Selenate Reductase. *Inorg. Chem. 45*, 2979–2988.
29. Bertero, M. G., Rothery, R. A., Palak, M., Hou, C., Lim, D., Blasco, F., Weiner, J. H., and Strynadka, N. C. J. (2003) Insights into the Respiratory Electron Transfer Pathway from the Structure of Nitrate Reductase A. *Nat. Struct. Biol. 10*, 681–687.
30. Raaijmakers, H. C. A., and Romão, M. J. (2006) Formate-reduced *E. coli* Formate Dehydrogenase H: The Reinterpretation of the Crystal Structure Suggests a New Reaction Mechanism. *J. Biol. Inorg. Chem. 11*, 849–854.
31. Lim, B. S., Willer, M. W., Miao, M., and Holm, R. H. (2001) Monodithiolene Molybdenum(V,VI) Complexes: A Structural Analogue of the Oxidized Active Site of the Sulfite Oxidase Enzyme Family. *J. Am. Chem. Soc. 123*, 8343–8349.
32. Groysman, S., Wang, J.-J., Tagore, R., Lee, S. C., and Holm, R. H. (2008) A Biomimetic Approach to Oxidized Sites in the Xanthine Oxidoreductase Family: Synthesis and Stereochemistry of Tungsten(VI) Analogue Complexes. *J. Am. Chem. Soc. 130*, 12794–12807.
33. Sung, K.-M., and Holm, R. H. (2001) Oxo Transfer Reactions Mediated by Bis(dithiolene)tungsten Analogues of the Active Sites of Molybdoenzymes in the DMSO Reductase Family: Comparative Reactivity of Tungsten and Molybdenum. *J. Am. Chem. Soc. 123*, 1931–1943.
34. Majumdar, A., Pal, K., and Sarkar, S. (2008) Selectivity of Thiolate Ligand and Preference of Substrate in Model Reactions of Dissimilatory Nitrate Reductase. *Inorg. Chem. 47*, 3393–3401.
35. Sugimoto, H., Tarumizu, M., Miyake, H., and Tsukube, H. (2008) Bis(dithiolene) Molybdenum Complex that Promotes Combined Coupled Electron-Proton Transfer and Oxygen Atom Transfer Reactions: A Water-Active Model of the Arsenite Oxidase Molybdenum Center. *Eur. J. Inorg. Chem.,* 4494–4497.
36. Lubitz, W., van Gastel, M., and Gaertner, W. (2007) Nickel Iron Hydrogenases. *Met. Ions Life Sci. 2*, 279–322.
37. Fontecilla-Camps, J. C., Volbeda, A., Cavazza, C., and Nicolet, Y. (2007) Structure-Function Relationships of the [NiFe]- and [FeFe]-Hydrogenase. *Chem. Rev. 107*, 4273–4303.
38. Lemon, B. J., and Peters, J. W. (2001) in *Handbook of Metalloproteins*, pp 738−751, Wiley & Sons, Ltd., Chichester, U.K.
39. Nicolet, Y., Cavazza, C., and Fontecilla-Camps, J. C. (2002) Fe-only Hydrogenases: Structure, Function, and Evolution. *J. Inorg. Biochem. 91*, 1–8.
40. Shima, S., Pilak, O., Vogt, S., Schick, M., Stagni, M. S., Meyer-Klaucke, W., Warkentin, E., Thauer, R. K., and Ermler, U. (2008) The Crystal Structure of [Fe]-Hydrogenase Reveals the Geometry of the Active Site. *Science 321*, 572–575.
41. Georgakaki, I. P., and Darensbourg, M. Y. (2004) in *Biocoordination Chemistry* (Que, L., Jr., and Tolman, W. A., Eds.) pp 549−568, Elsevier, Oxford, U.K.
42. Bouwman, E., and Reedijk, J. (2005) Structural and Functional Models Related to the Nickel Hydrogenases. *Coord. Chem. Rev. 249*, 1555–1581.
43. Liu, X., Ibrahim, S. K., Tard, C., and Pickett, C. J. (2005) Iron-only Hydrogenase: Synthetic, Structural, and Reactivity Studies of Model Compounds. *Coord. Chem. Rev. 249*, 1641–1652.
44. van der Vlugt, J. I., and Meyer, F. (2007) Synthetic Models for the Active Sites of Nickel-Containing Enzymes. *Met. Ions Life Sci. 2*, 181–240.
45. Canaguier, S., Artero, V., and Fontecave, M. (2008) Modelling NiFe Hydrogenases: Nickel-Based Electrocatalysts for Hydrogen Production. *Dalton Trans.,* 315–325.
46. Volbeda, A., and Fontecilla-Camps, J. C. (2005) Structural Bases for the Catalytic Mechanism of Ni-containing Carbon Monoxide Dehydrogenases. *J. Chem. Soc., Dalton Trans.,* 3443–3450.
47. Volbeda, A., Martin, L., Cavazza, C., Matho, M., Faber, B. W., Roseboom, W., Albracht, S. P. J., Garcin, E., Rousset, M., and Fontecilla-Camps, J. C. (2005) Structural Differences Between the Ready and Unready Oxidized States of [NiFe] Hydrogenases. *J. Biol. Inorg. Chem. 10*, 239–249.
48. Ogata, H., Hirota, S., Nakahara, A., Komori, H., Shibata, N., Kato, T., Kano, K., and Higuchi, Y. (2005) Process of [NiFe] Hydrogenase Eludicidated by High-Resolution X-Ray Analysis: Conversion of the Ready to the Unready State. *Structure 13*, 1635–1642.
49. Garcin, E., Vernede, X., Hatchikian, E. C., Volbeda, A., Frey, M., and Fontecilla-Camps, J. C. (1999) The Crystal Structure of a Reduced [NiFeSe] Hydrogenase Provides an Image of the Activated Catalytic Center. *Structure 7*, 557–566.
50. Sellman, D., Geipel, F., and Heinemann, F. W. (2002) (NEt_4) $[Fe(CN)_2(CO)(\text{'S3'})]$: An Iron Thiolate Complex Modeling the $[Fe(CN)_2(CO)(S\text{-}Cys)_2]$ Site of the [NiFe] Hydrogenase Centers. *Chem.—Eur. J. 8*, 958–966.
51. James, T. L., Cai, L., Muetterties, M. C., and Holm, R. H. (1996) Dihydrogen Evolution by Protonation Reactions of Nickel(I). *Inorg. Chem. 35*, 4148–4161.
52. Sellman, D., Geipel, F., and Moll, M. (2000) $[Ni(NHPPr^n_3)(\text{'S3'})]$, the First Nickel Thiolate Complex Modeling the Nickel Cysteinate Site and Reactivity of [NiFe] Hydrogenase. *Angew. Chem., Int. Ed. 39*, 561–563.
53. Li, Z., Ohki, Y., and Tatsumi, K. (2005) Dithiolato-Bridged Dinuclear Iron-Nickel Complexes $[Fe(CO)_2(CN)_2(\mu$-

$SCH_2CH_2CH_2S)Ni(S_2CNR_2)]^-$ Modeling the Active Site of [NiFe] Hydrogenases. *J. Am. Chem. Soc. 127*, 8950–8951.
54. Ohki, Y., Yasamura, K., Kuge, K., Tanino, S., Ando, M., Li, Z., and Tatsumi, K. (2008) Thiolate-bridged Dinuclear Iron(tris-carbonyl)-nickel Complexes Relevant to the Active Site of [NiFe] Hydrogenase. *Proc. Natl. Acad. Sci. U.S.A. 105*, 7652–7657.
55. Ogo, S., Kabe, R., Uehara, K., Kure, B., Nishimura, T., Menon, S. C., Harada, R., Fukuzumi, S., Higuchi, Y., Ohhara, T., Tamada, T., and Kuroki, R. (2007) A Dinuclear Ni(μ-H)Ru Complex Derived from H_2. *Science 316*, 585–587.
56. Pandey, A. S., Harris, T. V., Giles, L. J., Peters, J. W., and Szilagyi, R. K. (2008) Dithiomethylether as a Ligand in the Hydrogenase H-Cluster. *J. Am. Chem. Soc. 130*, 4533–4540.
57. Seyferth, D., Henderson, R. S., and Song, L. C. (1980) The Dithiobis(tricarbonyliron) Dianion: Improved Preparation and New Chemistry. *J. Organomet. Chem. 192*, C1–C5.
58. Singleton, M. L., Bhuvanesh, N., Reibenspies, J. H., and Darensbourg, M. Y. (2008) Synthetic Support of De Novo Design: Sterically Bulky [FeFe]-Hydrogenase Models. *Angew. Chem., Int. Ed. 47*, 9492–9495.
59. Stack, T. D. P., and Holm, R. H. (1988) Subsite-Differentiated Analogues of Biological $[4Fe\text{-}4S]^{2+}$ Clusters: Synthesis, Solution and Solid State Structures, and Subsite-Specific Reactions. *J. Am. Chem. Soc. 110*, 2484–2494.
60. Tard, C., Liu, X., Ibrahim, S. K., Bruschi, M., De Giola, L., Davies, S. C., Yang, X., Wang, L.-S., Sawers, G., and Pickett, C. J. (2005) Synthesis of the H-cluster Framework of Iron-only Hydrogenase. *Nature 433*, 610–613.
61. Capon, J.-F., Gloaguen, F., Schollhammer, P., and Talarmin, J. (2005) Catalysis of Electrochemical H_2 Evolution by Di-iron Subsite Models. *Coord. Chem. Rev. 249*, 1664–1676.
62. Heiden, Z. M., Zampella, G., De Gioia, L., and Rauchfuss, T. B. (2008) [FeFe]-Hydrogenase Models and Hydrogen: Oxidative Addition of Dihydrogen and Silanes. *Angew. Chem., Int. Ed. 47*, 9756–9759.
63. Beinert, H., Holm, R. H., and Münck, E. (1997) Iron-Sulfur Clusters: Nature's Modular, Multipurpose Structures. *Science 277*, 653–659.
64. Johnson, D. C., Dean, D. R., Smith, A. D., and Johnson, M. K. (2005) Structure, Function, and Formation of Biological Iron-Sulfur Clusters. *Annu. Rev. Biochem. 74*, 247–281.
65. Morales, R., Chron, M.-H., Hudry-Clergeon, G., Pétillot, Y., Norager, S., Medina, M., and Frey, M. (1999) Refined X-ray Structures of Oxidized, at 1.3 Å, and Reduced, at 1.17 Å, [2Fe-2S] Ferredoxin from the Cyanobacterium *Anabaena* PCC7119 Show Redox-Linked Conformational Changes. *Biochemistry 38*, 15764–15773.
66. Bönisch, H., Schmidt, C. L., Schäfer, G., and Ladenstein, R. (2002) The Structure of the Soluble Domain of an Archaeal Rieske Iron-Sulfur Protein at 1.1 Å Resolution. *J. Mol. Biol. 319*, 791–805.
67. Nielsen, M. S., Harris, P., Ooi, B.-L., and Christensen, H. E. M. (2004) The 1.5 Å Resolution Crystal Structure of $[Fe_3S_4]$-Ferredoxin from the Hyperthermophilic Archaeon *Pyrococcus furiosus*. *Biochemistry 43*, 5188–5194.
68. Fukuyama, K., Okada, T., Kakuta, Y., and Takahashi, Y. (2002) Atomic Resolution Structures of Oxidized [4Fe-4S] Ferredoxin from *Bacillus thermoproteolyticus* in Two Crystal Forms: Systematic Distortion of [4Fe-4S] Cluster in the Protein. *J. Mol. Biol. 315*, 1155–1166.
69. Rao, P. V., and Holm, R. H. (2004) Synthetic Analogues of the Active Sites of Iron-Sulfur Proteins. *Chem. Rev. 104*, 527–559.
70. Holm, R. H. (2004) Electron Transfer: Iron-Sulfur Clusters. In *Bio-coordination Chemistry* (Que, L., Jr., and Tolman, W. A., Eds.) pp 61−90, Elsevier, Oxford, U.K.
71. Link, T. A. (1999) The Structures of Rieske and Rieske-Type Proteins. *Adv. Inorg. Chem. 47*, 83–157.
72. Ballmann, J., Albers, A., Demeshko, S., Dechert, S., Bill, E., Bothe, E., Ryde, U., and Meyer, F. (2008) A Synthetic Analogue of Rieske-Type [2Fe-2S] Clusters. *Angew. Chem., Int. Ed. 47*, 9537–9541.
73. Brown, E. N., Friemann, R., Karlsson, A., Parales, J. V., Couture, M. M. J., Eltis, L. D., and Ramaswany, S. (2008) Determining the Rieske Cluster Reduction Potentials. *J. Biol. Inorg. Chem. 13*, 1301–1313.
74. Yoo, S. J., Angove, H. C., Burgess, B. K., Hendrich, M. P., and Münck, E. (1999) Mössbauer and Integer-Spin EPR Studies and Spin-Coupling Analysis of the $[4Fe\text{-}4S]^0$ Cluster of the Fe Protein of *Azotobacter vinelandii* Nitrogenase. *J. Am. Chem. Soc. 121*, 2534–2545.
75. Strop, P., Takahara, P. M., Chiu, H.-J., Angove, H. C., Burgess, B. K., and Rees, D. C. (2001) Crystal Structure of the All-Ferrous $[4Fe\text{-}4S]^0$ Form of the Nitrogenase Iron Protein from *Azotobacter vinelandii*. *Biochemistry 40*, 651–656.
76. Scott, T. A., Berlinguette, C. P., Holm, R. H., and Zhou, H.-C. (2005) Initial Synthesis and Structure of an All-Ferrous Analogue of the Fully Reduced $[Fe_4S_4]0$ Cluster of the Nitrogenase Iron Protein. *Proc. Natl. Acad. Sci. U.S.A. 102*, 9741–9744.
77. Deng, L., and Holm, R. H. (2008) Stabilization of Fully Reduced Iron-Sulfur Clusters by Carbene Ligation: The $[Fe_nS_n]^0$ Oxidation Levels (n = 4, 8). *J. Am. Chem. Soc. 130*, 9878–9886.
78. Chakrabarti, M., Deng, L., Holm, R. H., Münck, E., and Bominaar, E. L. (2009) Mössbauer, Electron Paramagnetic Resonance and Theoretical Study of a Carbene-Based All-Ferrous Fe_4S_4 Cluster: Electronic Origin and Structural Identification of the Unique Spectroscopic Site. *Inorg. Chem. 48*, (in press).
79. Dobbek, H., Gremer, L., Meyer, O., and Huber, R. (1999) Crystal Structure and Mechanism of CO Dehydrogenase: A Molybdo Iron-Sulfur Flavoprotein Containing *S*-selanylcysteine. *Proc. Natl. Acad. Sci. U.S.A. 96*, 8884–8889.
80. Ragsdale, S. W., and Kumar, M. (1996) Nickel-Containing Carbon Monoxide Dehydrogenase/Acetyl-CoA Synthase. *Chem. Rev. 96*, 2515–2539.
81. Lindahl, P. A., and Graham, D. E. (2007) Acetyl-coenzyme A Synthases and Nickel-Containing Carbon Monoxide Dehydrogenases. *Met. Ions Life Sci. 2*, 357–415.
82. Lindahl, P. A. (2008) Implications of a Carboxylate-Bound C-Cluster Structure of Carbon Monoxide Dehydrogenase. *Angew. Chem., Int. Ed. 47*, 4054–4056.
83. Dobbek, H., Gremer, L., Kiefersauer, R., Huber, R., and Meyer, O. (2002) Catalysis at a Dinuclear [CuSMo(=O)OH] Cluster in a CO Dehydrogenase Resolved at 1.1-Å Resolution. *Proc. Natl. Acad. Sci. U.S.A. 99*, 15971–15976.
84. Gourley, C., Nielsen, D. J., White, J. M., Knottenbelt, S. Z., Kirk, M. L., and Young, C. G. (2006) Paramagnetic Active Site Models for the Molybdenum-Copper Carbon Monoxide Dehydrogenase. *J. Am. Chem. Soc. 128*, 2164–2165.
85. Takuma, M., Ohki, Y., and Tatsumi, K. (2005) Sulfido-Bridged Dinuclear Molybdenum-Copper Complexes Related to the Active Site of CO Dehydrogenase: $[(dithiolate)Mo(O)S_2Cu(SAr)]^{2-}$ (dithiolate = $1,2\text{-}S_2C_6H_4$, $1,2\text{-}S_2C_6H_2\text{-}3,6\text{-}Cl_2$, $1,2\text{-}S_2C_2H_4$). *Inorg. Chem. 44*, 6034–6043.
86. Zhou, J., Raebiger, J. W., Crawford, C. A., and Holm, R. H. (1997) Metal Ion Incorporation Reactions of the Cluster $[Fe_3S_4(LS_3)]^{3-}$, Containing the Cuboidal $[Fe_3S_4]^0$ Core. *J. Am. Chem. Soc. 119*, 6242–6250.
87. Panda, R., Berlinguette, C. P., Zhang, Y., and Holm, R. H. (2005) Synthesis of MFe_3S_4 Clusters Containing a Planar M^{II} Site (M = Ni, Pd, Pt), a Structural Element in the C-Cluster of Carbon Monoxide Dehydrogenase. *J. Am. Chem. Soc. 127*, 11092–11101.
88. Sun, J., Tessier, C., and Holm, R. H. (2007) Sulfur Ligand Substitution at the Nickel(II) Sites of Cubane-Type and Cubanoid $NiFe_3S_4$ Clusters Relevant to the C-Clusters of Carbon Monoxide Dehydrogenase. *Inorg. Chem. 46*, 2691–2699.
89. Dobbek, H., Svetlitchnyi, V., Liss, J., and Meyer, O. (2004) Carbon Monoxide Induced Decomposition of the Active Site [Ni-4Fe-5S] Cluster of CO Dehydrogenase. *J. Am. Chem. Soc. 126*, 5382–5387.
90. Jeoung, J.-H., and Dobbek, H. (2007) Carbon Dioxide Activation at the Ni,Fe-Cluster of Anaerobic Carbon Monoxide Dehydrogenase. *Science 318*, 1461–1464.
91. Howard, J. B., and Rees, D. C. (1996) Structural Basis of Biological Nitrogen Fixation. *Chem. Rev. 96*, 2965–2982.
92. Howard, J. B., and Rees, D. C. (2006) How Many Metals Does It Take to Fix N_2? A Mechanistic Overview of Biological Nitrogen Fixation. *Proc. Natl. Acad. Sci. U.S.A. 103*, 17088–17093.
93. Peters, J. W., Stowell, M. H. B., Soltis, S. M., Finnegan, M. G., Johnson, M. K., and Rees, D. C. (1997) Redox-Dependent Structural Changes in the Nitrogenase P-Cluster. *Biochemistry 36*, 1181–1187.
94. Mayer, S. M., Lawson, D. M., Gormal, C. A., Roe, S. M., and Smith, B. E. (1999) New Insights into Structure-function Relationships in Nitrogenase: A 1.6 Å X-ray Crystallographic Study of *Klebsiella pneumoniae* MoFe-protein. *J. Mol. Biol. 292*, 871–891.
95. Einsle, O., Tezcan, F. A., Andrade, S. L. A., Schmid, B., Yoshida, M., Howard, J. B., and Rees, D. C. (2002) Nitrogenase MoFe-

Protein at 1.16 Å Resolution: A Central Ligand in the FeMo-Cofactor. *Science 297*, 1696–1700.

96. Lee, S. C., and Holm, R. H. (2003) Speculative Synthetic Chemistry and the Nitrogenase Problem. *Proc. Natl. Acad. Sci. U.S.A. 100*, 3595–3600.
97. Lee, S. C., and Holm, R. H. (2004) The Clusters of Nitrogenase: Synthetic Methodology in the Construction of Weak-Field Clusters. *Chem. Rev. 104*, 1135–1157.
98. Berlinguette, C. P., Miyaji, T., Zhang, Y., and Holm, R. H. (2006) Precursors to Clusters with the Topology of the P^N Cluster of Nitrogenase: Edge-Bridged Double Cubane Clusters $[(Tp)_2Mo_2Fe_6S_8L_4]^z$. Synthesis, Structures, and Electron Transfer Series. *Inorg. Chem. 45*, 1997–2007.
99. Zhang, Y., and Holm, R. H. (2003) Synthesis of a Molecular $Mo_2Fe_6S_9$ Cluster with the Topology of the P^N Cluster of Nitrogenase by Rearrangement of an Edge-Bridged $Mo_2Fe_6S_8$ Double Cubane. *J. Am. Chem. Soc. 125*, 3910–3920.
100. Zuo, J.-L., Zhou, H.-C., and Holm, R. H. (2003) Vanadium-Iron-Sulfur Clusters Containing the Cubane-Type $[VFe_3S_4]$ Core Unit: Synthesis of a Cluster with the Topology of the P^N Cluster of Nitrogenase. *Inorg. Chem. 42*, 4624–4631.
101. Osterloh, F., Sanakis, Y., Staples, R. J., Münck, E., and Holm, R. H. (1999) A Molybdenum-Iron-Sulfur Cluster Containing Structural Elements Relevant to the P-Cluster of Nitrogenase. *Angew. Chem., Int. Ed. 38*, 2066–2070.
102. Osterloh, F., Achim, C., and Holm, R. H. (2001) Reduced Molybdenum-Iron-Sulfur Clusters of Nuclearities Eight and Sixteen, Including a Topological Analogue of the P-Cluster of Nitrogenase. *Inorg. Chem. 40*, 224–232.
103. Ohki, Y., Ikagawa, Y., and Tatsumi, K. (2007) Synthesis of New [8Fe-7S] Clusters: A Topological Link between the Core Structures of P-Cluster, FeMo-co and FeFe-co of Nitrogenase. *J. Am. Chem. Soc. 129*, 10457–10465.
104. Kukchar, J., and Hausinger, R. P. (2004) Biosynthesis of Metal Sites. *Chem. Rev. 104*, 509–525.
105. Dos Santos, P. C., Dean, D. R., Hu, Y., and Ribbe, M. W. (2004) Formation and Insertion of the Nitrogenase Iron-Molybdenum Cofactor. *Chem. Rev. 104*, 1159–1173.
106. Hu, Y., Fay, A. W., Lee, C. C., Yoshizawa, J., and Ribbe, M. W. (2008) Assembly of Nitrogenase MoFe protein. *Biochemistry 47*, 3973–3981.

BI900044E